In-Situ Precipitation of Silver Chloride on Alumina Porous Lattices for Potable Water Disinfection

Sofia K. Fanourakis[*],
Seabrook Solutions, LLC, NASA Ames Research Center, Moffett Field, CA, 94035, USA

Alan C. Swavely[†],
North Carolina State University, Raleigh, NC 27606, USA

Tra-My Justine Richardson[‡], Michael Flynn[§], Lance Delzeit[**],
NASA Ames Research Center, Moffett Field, CA, 94035, USA

Joe Cesarano[††], Alex Valdez[‡‡]
Robocasting Enterprises LLC, Albuquerque, NM, 87109, USA

Avi Gerber[§§],
University of California Los Angeles, Los Angeles, CA 90095, USA

Andrew Nguyen[§§],
University of California Santa Cruz, Santa Cruz, CA 95064, USA

and

Sajjad Bigham[***]
North Carolina State University, Raleigh, NC 27606, USA

As the National Aeronautics and Space Administration (NASA) plans for both transit and planetary missions further into space, access to potable water is a vital component in sustainable life support. Currently, potable water aboard the International Space Station is disinfected using iodine to stabilize the water's shelf life. However, prolonged exposure to iodine-treated water can increase the risk of autoimmune thyroid disorders (AITDs). As a long-term alternative, NASA is investigating the use of silver ions (Ag^+) for spacecraft potable water disinfection. This paper discusses the development and testing of in-situ precipitated silver chloride (AgCl) on porous alumina 3D-printed lattices manufactured using robocasting techniques. The porous alumina rods had an estimated porosity of 65%, which allowed the structures to wick the precursor solutions and provided a high internal surface area for AgCl coating and passive silver dosing. The lattices were coated using alternating silver nitrate and sodium chloride (NaCl) infiltration methods and tested using a flow-through system at flow rates between 0.05 and 0.25 L/min. Effluent Ag^+ concentration was measured using a silver ion selective electrode. Lattice samples with cumulative AgCl loading values of 5.45 and 6.06 g produced average effluent concentrations within the desired 200 to 400 ppb range at a flow rate of 0.1 L/min. Flow rate testing showed a nonlinear decrease in outlet Ag^+ concentration

[*] Research Scientist, Bioengineering Branch, MS-239-15, Moffett Field, CA 94035, USA.
[†] Ph.D. Student, Mechanical and Aerospace Engineering, North Carolina State University, NC 27606, USA.
[‡] Research Physical Scientist, Bioengineering Branch, MS-239-15, Moffett Field, CA 94035, USA.
[§] Physical Scientist, Bioengineering Branch, MS-239-15, Moffett Field, CA 94035, USA.
[**] Physical Scientist, Bioengineering Branch, MS-239-15, Moffett Field, CA 94035, USA.
[††] President, 5660 Pino Avenue NE, Albuquerque, NM 87109.
[‡‡] Engineer, 5660 Pino Avenue NE, Albuquerque, NM 87109.
[§§] Engineering Intern, Bioengineering Branch, MS-239-15, Moffett Field, CA 94035, USA.
[***] Associate Professor, Mechanical and Aerospace Engineering, North Carolina State University, NC 27606, USA.

with increasing flow rate. Computational fluid dynamics modeling was also performed to investigate the effects of flow rate and lattice geometry on Ag^+ release behavior. The results support continued development of In-Situ AgCl-coated porous alumina lattices as a passive alternative to iodine-based spacecraft water disinfection systems.

Trade names and trademarks and company names are used in this report for identification only. Their usage does not constitute an official endorsement, either expressed or implied, by the National Aeronautics and Space Administration.

Acronyms and Nomenclature

Ag^+	=	silver ion
$AgCl$	=	silver chloride
$AgNO_3$	=	silver nitrate
AITDs	=	autoimmune thyroid disorders
ARC	=	Ames Research Center
g	=	grams
ISE	=	Ion Selective Electrode
ISS	=	International Space Station
L	=	liters
min	=	minute
NaCl	=	sodium chloride
NASA	=	National Aeronautics and Space Administration
ppb	=	parts per billion
psig	=	pounds per square inch gauge
ρ	=	Density
$\vec{u}$	=	Velocity
g	=	Gravitational acceleration
p	=	Pressure
μ	=	Viscosity
C	=	Species concentration
S	=	Source term
Re	=	Reynolds number
Sc	=	Schmidt number
k	=	Mass transfer coefficient
A	=	Interfacial area
D	=	Binary diffusion coefficient
d_h	=	Hydraulic diameter
α	=	Tuning factor
d_p	=	Particle diameter
ε	=	Porosity

I. Introduction

Silver is widely used as a water disinfectant due to its antibacterial and antiviral properties. In recent years, the National Aeronautics and Space Administration (NASA) has been interested in replacing its preexisting passive iodine dosing system with a silver dosing system for long duration missions. While iodine is the currently used disinfection method on the International Space Station (ISS), it can lead to an increased risk of developing autoimmune thyroid disorders (AITDs) with prolonged exposure [1–3]. Thus, iodine requires removal from water prior to ingestion, which requires additional hardware and increases the complexity of the potable water system.

Currently, Russian astronauts are disinfecting their water with silver [4]. However, their system is what we consider an active dosing system. They run a low current through silver electrodes that slowly release silver ions. In order to keep much of the same infrastructure as the iodine dosing system, NASA is currently exploring methods to passively dose silver. The silver dosing being explored should adhere to the following performance parameters to maintain the microbial control of the system in accordance with typical spacecraft potable water specifications as outlined in [5,6].

- Maintain 200 to 400 ppb of silver in the water at flow rates of 0.10 to 0.15 L/min.
- Operate at ambient temperature.
- Operate at pH ranges between 4.5 - 9.0.
- Be able to handle system pressures up to 30 psig.

One of the passive dosing technologies currently being investigated by NASA is the Silver Foam, which utilizes a silver compound nanocomposite polyurethane foam to release silver ions into water at a concentration of 200 to 400 ppb [7]. While the Silver Foam technology is also capable of passively dosing silver into potable water, the technology discussed in this work can provide an alternative to the foam that is an unlikely source of total organic carbon and is highly modifiable, allowing the lattice geometry, porosity, rod diameter, length, and AgCl loading to be tailored to mission-specific flow rate and silver dosing requirements. The system explored in this paper utilizes silver chloride (AgCl) coated 3D-printed ceramic lattices. Similar to the zeolite lattices used in the MultiSORB project [8,9], NASA engineers theorized that we could re-purpose a similar structure to passively dose silver. The grid patterns in the lattice

are optimally designed to maximize the interior surface area and minimize the volume, thus providing ample surface area for precipitating AgCl onto the lattice structures. The lattice geometry was selected to maximize the surface-area-to-volume ratio while maintaining acceptable flow resistance and structural integrity. Initial feasibility testing demonstrated that the available surface area was sufficient to produce effluent Ag^+ concentrations within the desired 200 to 400 ppb range at a flow rate of 0.1 L/min [9]. Coating the lattices with AgCl and flowing water at 0.1 L/min through the coated lattice, should be able to passively introduce enough silver ions into the water to disinfect it. To test this theory, a feasibility study was performed on the coated lattice structures, showing promising results [9]. Namely, a lattice coated with 2.8 g AgCl resulted in 268 ppb Ag^+ at a flow rate of 0.1 L/min [9]. Herein, we further investigate the use of AgCl-coated 3D-printed ceramic lattices for passively dosing water with Ag^+.

II. Methodology

A. AgCl-coated porous alumina lattice manufacture and coating

The lattice structures were manufactured and coated with AgCl by Robocasting Enterprises LLC using a previously reported method [9]. Briefly, porous alumina lattices were 3D printed using the additive manufacturing technique known as robocasting. Each strut was 1.2 mm in diameter, and the structure had in-plane gaps of 1.08 mm and was stacked with gaps of approximately 0.97 mm. Fugitive polymer beads were used to control the internal porosity to tens of microns. Using the high wicking ability of the alumina structures, a 3 M solution of either $AgNO_3$ or NaCl was used to soak each sample, which was subsequently dried. Once dried, a solution of 3 M NaCl or $AgNO_3$ was used to precipitate AgCl on the surface and inside the pores of the alumina lattice samples. SEM images were acquired to assess the effectiveness of the coating. Robocasting Enterprises LLC supplied NASA Ames Research Center (ARC) with two sets of 6 lattice structures (Figure 1), where lattice samples 1-6 were coated by soaking the lattices in $AgNO_3$ first and then adding NaCl to precipitate AgCl, and lattice samples 7-12 were coated by soaking in NaCl first and then adding $AgNO_3$. AgCl loading was estimated based on the weight of the lattices before and after the coating procedure. Table 1 shows the estimated loading value for each lattice sample. We should note that the coating process is still being fine-tuned, and additional experiments will be carried out to test the effectiveness of the coatings.



Figure 1. Two modules containing the Ag-coated lattice samples 1-6 and 7-12 delivered to ARC by Robocasting Enterprises LLC.

Table 1. Estimated AgCl loading for each lattice sample.

Sample	1	2	3	4	5	6	7	8	9	10	11	12
AgCl (g)	1.63	1.10	1.07	2.72	2.10	1.24	1.81	1.71	1.92	1.94	1.68	1.26

B. AgCl-coated porous alumina lattice testing

To test the functionality of the AgCl-coated lattices, a simple flow-through system was implemented (Figure 2) and effluent Ag+ concentration was measured using a silver/sulfide ion selective probe (ISE). Three lattices from each canister were selected. In a typical experiment, the ISE probe was calibrated using standard solutions of 40, 80, 120, 300, 450, and 650 ppb of silver made from a stock solution of 1000 ppb, which was diluted from a 1 g/L silver standard (Sigma Aldrich, 12818). Each calibration standard contained a low-level ionic strength adjuster (ISA) at a 100:1 ratio. Low level ISA was prepared prior to the experiment by diluting 20 mL into a 100 mL volumetric flask with deionized water.

When testing lattices 4-6, while the ISE probe was being calibrated, the canister was filled and ran at 0.1

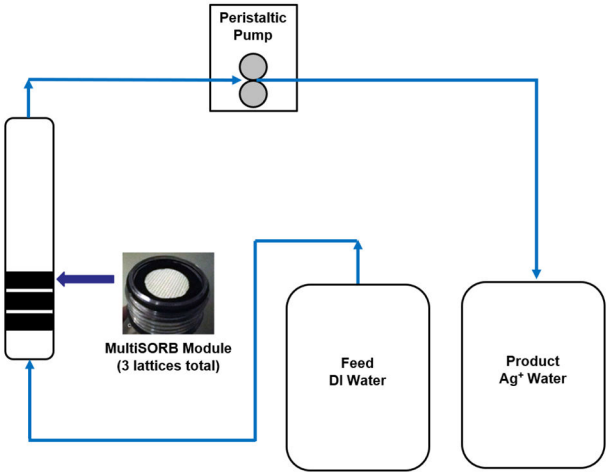


Figure 2. AgCl-loaded alumina lattice test setup.

L/min. Samples were taken approximately every 10 mins, weighed, and an amount of 100th of the weight of low-level ISA was added prior to measurement with the ISE probe. The experiment was repeated on three separate days to test repeatability. When testing lattices 7-9, the peristaltic pump was set to 0.05 L/min initially, and the flow rate was increased to up to 0.25 L/min. Samples were taken every 5 to 10 mins, and each sample was weighed, and an appropriate amount of low-level ISA was added prior to each measurement. This data was acquired not only to assess the performance of the lattices at different flow rates, but also to provide data to evaluate the validity of the flow dynamics model being developed by North Carolina State University.

C. Computational modeling approach

In conjunction with experimental evaluation, detailed, multispecies computational fluid dynamics (CFD) modeling was performed using the finite-volume method to examine the potential of passive silver ion (Ag+) dosing via a 3D-printed AgCl-coated alumina lattice reactor. A continuum-based approach was utilized to model both the flow and mass transport processes within the water domain using the following assumptions:

1. The water flow through the solid reactor structure is laminar and incompressible.
2. The water solution is highly diluted in Ag^+ and Cl^-. Therefore, the properties of the water mixture are the same as those of pure water.
3. As the solubility of AgCl in water is so small, the enthalpy of dissolution is ignored.
4. The dissolution of silver and chloride ions at the AgCl-coated alumina surface is fast enough to maintain the concentrations of Ag^+ and Cl^- at saturation levels determined by the solubility product constant (K_{sp}) at 25°C.

The Navier-Stokes equations, along with species transport and energy equations, were applied to determine the spatial distribution of the Ag^+ concentration along the 3D lattice reactor length. The continuity, momentum, and species transport equations can be written as:

$$\frac{\partial \rho_w}{\partial t} + \nabla \cdot (\rho_w \vec{u}) = 0 \tag{1}$$

$$\rho_w \left(\frac{\partial \vec{u}}{\partial t} + (\vec{u} \cdot \nabla)\vec{u}\right) = -\nabla p + \mu_w \nabla^2 \vec{u} \tag{2}$$

$$\frac{\partial (\rho_w C_{Ag+})}{\partial t} + \nabla \cdot \left(\rho_w \vec{u} C_{Ag+}\right) = -\nabla \cdot (D_{i,w} \nabla C_{Ag+}) + S_{Ag+} \tag{3}$$

where ρ_w is the water density, $\vec{u}$ is the velocity vector, p is the pressure, μ_w is the water viscosity, C_{Ag+} is the mass fraction of Ag^+, and $D_{i,w}$ is the binary diffusion coefficient. S_{Ag+} is the Ag^+ source term within the porous media zone of individual 3D-printed AgCl-coated alumina rods. The linear driving force formulation used in Eq. (4) is commonly applied in dissolution and mass transfer modeling to approximate interfacial species transport between solid and fluid phases. [10]. The source term is defined as a linear driving force between the solubility limit of Ag+ and the local fluid concentration of Ag^+, adapted from [10] as follows:

$$S_{Ag+} = k_m A \rho_{H_2O} (C^*_{Ag+} - C_f) \tag{4}$$

where k_m, A, C^*_{Ag+}, and C_f represent the mass transfer coefficient [m/s], the specific surface area [m^2/m^3], the equilibrium mass fraction of Ag+ at the AgCl-coated alumina interface, and the mass fraction [g_{Ag+}/g_{water}] of Ag+ in the water solution, respectively. It should be noted that C^*_{Ag+} was obtained from the solubility product constant (K_{sp}) at 25°C.

The external and internal mass transfer coefficient correlations were adapted from conventional porous-media and packed-bed mass transfer relationships, Eq. (5)-(7) [11,12]. The effective mass transfer coefficient [m/s], k_{eff}, is a function of the external (k_e) and internal (k_i) mass transfer coefficients, scaled by an empirically determined correction factor (α), as follows:

$$k_{eff} = \alpha \frac{k_i k_e}{k_i + k_e} \tag{5}$$

where the external and internal mass transfer coefficients are:

$$k_e = 0.023 Re^{0.8} Sc^{0.4} \tag{6}$$

$$k_i = D_{eff} \frac{1-\varepsilon}{A L_c^2} \quad (7)$$

where Re, Sc, D_{eff}, ε, and L_c are Reynolds number [-], Schmidt number [-], effective diffusion coefficient [m^2/s] within porous rods, rod porosity [-], and characteristic length [m], respectively.

By defining the silver dissolution source term in this manner, two key assumptions are made. First, the lattice is assumed to be evenly infiltrated with AgCl throughout the internal volume of porous rods, as opposed to an external surface coating. Second, the lattice acts as an infinite Ag^+ source with no physical limit. Although the infinite Ag^+ source assumption does not significantly affect the initial transient outlet concentration predictions presented in this study, depletion of AgCl over long-duration operation would eventually influence dosing behavior and therefore requires additional depletion-tracking logic in future model development. Based on the evaluation of experimental samples, the first assumption does not pose appreciable risk to the reliability of this model. The second assumption does not directly affect the model's fidelity for initial values, but it should be noted that future longevity studies will require additional logic to track the mass of AgCl dissolved rather than the immediate concentration alone. Also, experimental data collected by NASA Ames Research Center were used to determine the correction factor, considering the outlet Ag^+ concentration at a single flow rate of 0.1 LPM. Symmetry boundary conditions were applied to minimize the computational cost. Ansys Fluent was used as the primary CFD solver. The porous lattice properties and flow conditions were defined to mirror experimental conditions. A mesh independence study was performed to ensure the simulation results are independent of the mesh employed. Upon the mesh independent study, a tetrahedral mesh with a 50-micron element size was selected. The porosity and permeability of the lattice rods is 65% and 1.34×10^{-13} m^2, respectively [13]. Permeability was estimated using porous media correlations [12] and measured directly according to the procedure outlined in [14].

III. Results and Discussion

A. AgCl-coated porous alumina lattice testing

Lattice samples 4-6 were tested using a flow rate of 0.1 L/min on three separate days. Each day, samples were taken every 5 to 10 mins until confident that the effluent concentration had reached a steady state (Figure 3a). The first day they were run, Ag^+ effluent concentrations ranged from 359 to 401 ppb with an average value of 386 ppb Ag^+ and a standard deviation of 12 ppb. The first day average was higher than the second and third days, which had average Ag^+ effluent concentrations of 338 ± 13 ppb and 340 ± 5 ppb, respectively, likely due to AgCl that was not as strongly adhered to the alumina surface, thus dissolving more readily into the solution. Values for the second and third days were more consistent, indicating that the system may require some initial run time to reach a steadier effluent Ag^+ concentration.

To better assess the variability in the data, ensemble averaging was performed for time points that were within 2 mins of each other (Figure 3b). Most data points presented with low standard deviation, with the majority having standard deviation values of 16 to 20 ppb. Over the three days of testing, lattice samples 4-6 had an average effluent Ag^+ concentration of 354 ± 25 ppb, which is well within the 200 to 400 ppb desired range. These samples had a cumulative AgCl loading of 6.06 g, which calculates to 58.4 ppb of Ag^+ released per gram of AgCl loading. This value provides an estimate of silver dosing efficiency relative to AgCl loading and may be useful for predicting approximate Ag^+ release concentrations for future lattice configurations.

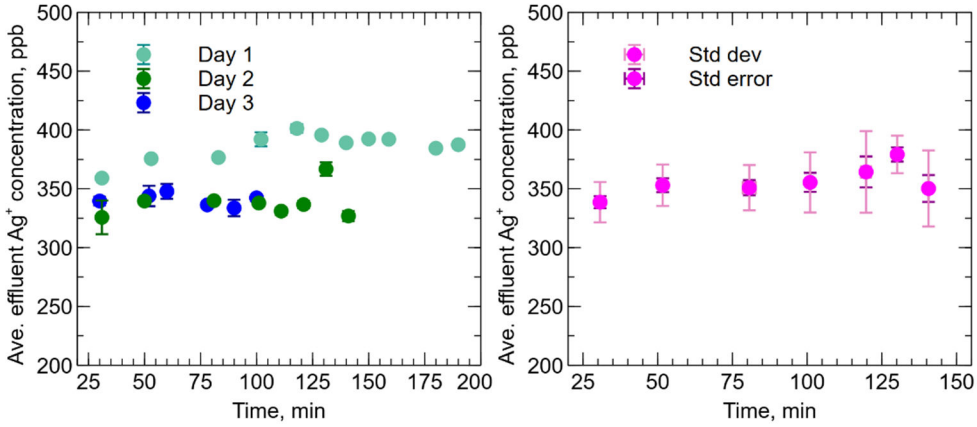


Figure 3. Effluent Ag^+ concentration over time for lattices 4 through 6 when using a flow rate of 0.1 L/min. a) Test results separated by day, and b) three-day averages with standard deviation and standard error.

Lattice samples 7-9 were then selected for testing the effects of flow rate, as there was less variability in AgCl loading between samples in this batch of coated lattices. A more consistent AgCl loading was thought to yield more reproducible results when testing different lattice samples. With a cumulative loading of 5.45 g AgCl, lattice samples 7-9 were initially estimated to be able to provide 318 ppb of Ag^+ at 0.1 L/min. This estimate was based on the Ag^+ effluent concentration per gram of AgCl loading from testing lattice samples 4-6.

The first flow rate test (Figure 4 – green data points) was run similarly to lattice samples 4-6, where the canister was filled at a flow rate of 0.1 L/min. Then, the flow rate was changed to 0.05 L/min, and samples were collected and tested every 5 to 10 mins. Figure 4 shows the average value at each flow rate, where at least three stable data points were used to ensure the values represent the steady state concentration at each flow rate. Initially, the values at the low flow rates (0.05 and 0.1 L/min) were lower than expected, showing a linear relationship between flow rate and Ag^+ concentration (Figure 4 – green data points). This was unexpected since, when no flow is present, Ag^+ is expected to reach its saturation point in water (~1450 ppb); thus, as diffusion forces become more dominant with decreasing flow rate, Ag^+ concentration is expected to be closer and closer to the saturation concentration. We theorized that a reason for this discrepancy could be the presence of bubbles. Bubbles would prevent water from making full contact with the full surface area available, thus reducing the amount of silver dissolved in water. A simple solution was to allow the lattices to soak in water over a period of 2.5 days. Upon re-testing lattice samples 7-9 after the soak period, the Ag^+ effluent concentration at 0.1 L/min was much closer to the expected value of 318 ppb (effluent Ag^+ concentration increased from 279 ± 2 ppb to 317 ± 4 ppb when samples were presoaked). Additionally, the relationship between Ag^+ concentration and flow rate was found to be non-linear as initially expected (Figure 4 – blue data points). Curiously, at the higher flow rate (> 0.15 L/min), the impact of bubbles was not evident. This is likely due to the flow dynamics of the lattices that vastly depend on the overall structure as well as the porosity of the alumina.

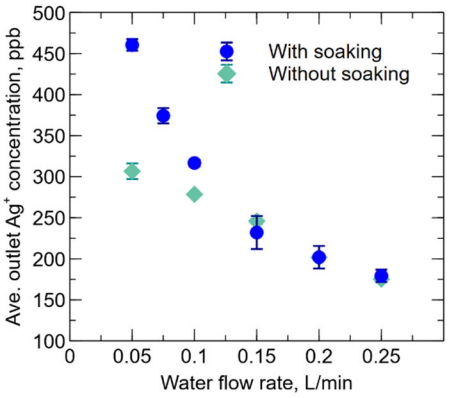


Figure 4. Lattice samples 6-9 flow rate testing without pre-soaking the structures and after soaking for 2.5 days.

An interesting observation was that bubbles were not an issue when testing lattice samples 4-6. The effluent Ag^+ concentration did not significantly change with repeat experiments, and there were no significant fluctuations observed in the data at different timepoints. The main difference between these two sets of samples was the order in which the precursor solutions were added to coat the alumina with AgCl. In samples 4-6, $AgNO_3$ was added first, whereas in samples 7-9, NaCl was added first. Performing a quick water drop test showed that the surface of samples 4-6 is more hydrophilic than that of samples 7-9, where a drop of water took seconds to absorb into the structure. This indicates a difference in how the structures are coated and will require more thorough testing. While both methods yield effluent Ag^+ concentrations of roughly 58 ppb/g of coated AgCl, the difference in coating methods could result in different longevity, where one method could lead to faster depletion of AgCl than the other.

B. Computational results

Figure 5 shows the experimental and model average outlet concentrations of Ag^+ ions as a function of water flow rate. The water flow rate varies from 0.05 to 0.25 L/min, corresponding to Reynolds numbers ranging from 29 to 143, which indicates laminar flow conditions. The relationship between outlet Ag^+ concentration and flow rate is nonlinear in nature and shows a decrease in outlet concentration as flow rate increases. For example, as flow rate increases from 0.1 to 0.25 L/min (by 150%), outlet concentration decreases from 316.7 to 179.3 ppb (by 43%). Figure 6 shows the corresponding contours of Ag^+ concentration at flow rates of 0.1 and 0.25 L/min. The average hydraulic residence time within the porous lattice structure decreased as the flow rate increased. As the flow rate increased from 0.05 to 0.25 L/min, the reduced liquid-solid contact time limited the ability of the flowing water to approach equilibrium AgCl saturation conditions within the porous structure. The measured outlet Ag^+ concentrations remained below the theoretical equilibrium

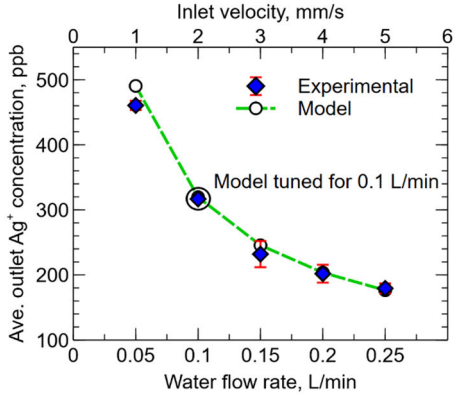


Figure 5. Experimental and model average outlet mass fractions of Ag+ ions as a function of water flow rate.

solubility concentration of AgCl in pure water (~900 ppb at room temperature), which suggests that the system operated under non-equilibrium and mass-transfer-influenced conditions rather than equilibrium-limited dissolution conditions. The decrease in the outlet Ag^+ concentration with flow rate occurs even though the mass transfer coefficient, Ag^+ release rate, and the total number of Ag^+ ions released into the water stream all increase at higher water flow rates due to the thinning of the mass transfer boundary layer. Although higher flow rates enhanced the Ag^+ release rate, this increase did not scale proportionally with the additional water introduced into the system, resulting in a lower outlet concentration of Ag^+ ions at higher flow rates. Gas bubble accumulation within portions of the porous lattice may have additionally reduced the effective wetted AgCl surface area available for dissolution and contributed to localized reductions in liquid-solid contact area. In other words, although higher flow rates enhance the Ag^+ release rate, this increase does not scale proportionally with the additional water introduced, resulting in a lower outlet concentration of Ag^+ ions. Additionally, there is a good agreement between the model and experimental results, with a maximum deviation of less than 6.5% at the lowest flow rate examined. The higher deviation between the model and experimental data at this condition may be attributed to increased experimental uncertainty at low flow rates, as well as uncertainties in the modeled mass transfer coefficient.

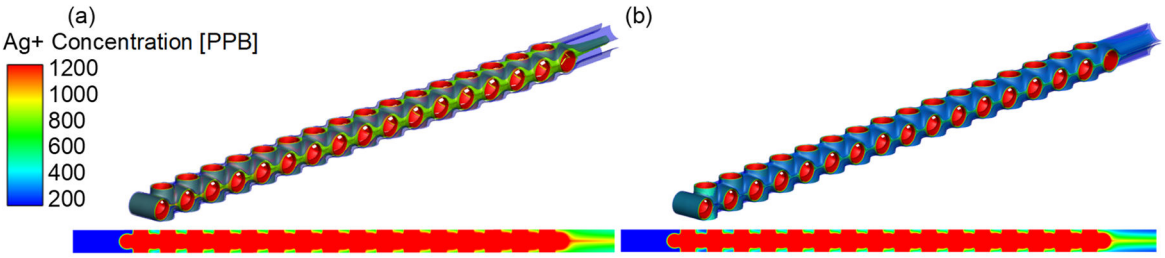


Figure 6. Contours of Ag+ concentration at flow rates of (a) 0.1 and (b) 0.25 L/min.

Figure 7 shows the average outlet mass fraction of Ag^+ ions along the reactor length at different rod diameters and a fixed flow rate of 0.1 L/min According to Eqs. (4)–(7), decreasing rod diameter increases the specific surface area available for AgCl dissolution and reduces characteristic diffusion length scales, thereby increasing the effective Ag^+ mass transfer rate into the flowing water. Similarly, increasing flow rate enhances the external mass transfer coefficient through higher Reynolds number, resulting in increased Ag^+ dissolution flux. However, because volumetric throughput increases more rapidly than the total Ag^+ release rate, the outlet Ag^+ concentration decreases with increasing flow rate. For a reactor with a fixed rod diameter and specific surface area, the mass fraction of Ag^+ ions almost linearly increases along the reactor length, indicating that the growth in the thickness of the Ag^+ mass boundary layer along the reactor length does not substantially limit the Ag^+ release rate. For instance, at a rod diameter of 2 mm, the concentration of the Ag^+ ions increases from 0 at the inlet to 242 ppb at a reactor length of 36 mm. Additionally, as the rod diameter decreases, the outlet concentration of the Ag^+ ions increases with the reactor surface-area-to-volume ratio due to higher Ag^+ dissolution surface areas. For instance, when the reactor surface-area-to-volume ratio increases from 1.95 to 5.24 m^2/m^3 (corresponding to rod diameters of 2.4 and 0.8 mm), the outlet Ag^+ mass fraction increases from 215 to 395 ppb.

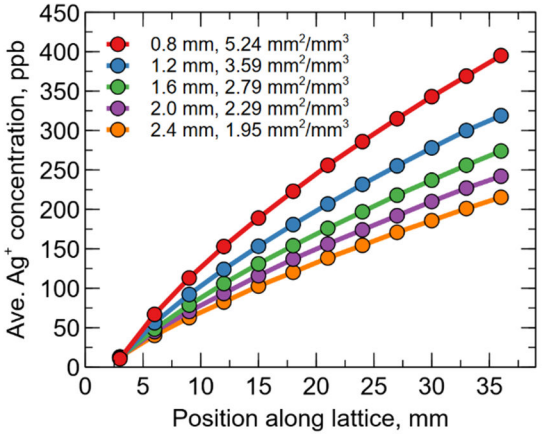


Figure 7. Average outlet mass fraction of Ag^+ ions along the reactor length at different rod diameters and a fixed flow rate of 0.1 L/min.

IV. Future Work

Long-duration flow testing and recirculation studies will be conducted in the future to evaluate the depletion rate of AgCl over time and to determine the operational lifetime of the lattices under mission-relevant conditions. In the more immediate future, lattice samples from each coating method (AgNO3 first and NaCl first) will undergo accelerated long-duration testing, where water will be passed through the lattice samples at a rate of 0.1 L/min continuously over the course of a month, such that more than 2800 L of water is treated with silver. At a continuous flow rate of 0.1 L/min, a single lattice module would process approximately 144 L/day or 52,560 L/year. Assuming a

potable water consumption rate of approximately 3–5 L/day per crew member, this corresponds to the annual potable water needs of approximately 28–48 crew members, although actual mission usage would depend on system architecture, water recirculation strategy, and allowable Ag^+ depletion limits. The longevity of the lattices will be assessed based on the maximum volume of water that can be treated with 200 to 400 ppb of Ag+. Then, the dormancy behavior of the lattices will be evaluated by cycling between running the system for multiple days and turning it off for several days. During this time, the ability of the system to use recirculated water will also be examined. The intended application includes both single-pass and partially recirculated spacecraft potable water systems were maintaining residual Ag^+ concentrations within the desired antimicrobial range is necessary for microbial control. Additionally, the computational model will be extended to study the effect of rod porosity, rod permeability, rod arrangement, lattice length, and coating uniformity on the outlet Ag+ concentration. The current modeling approach focuses on predicting the initial Ag^+ release behavior and therefore uses several simplifying assumptions, including uniform AgCl infiltration throughout the porous rods, saturation-limited dissolution behavior, and an effectively infinite Ag^+ source. While these assumptions are reasonable for evaluating the initial dosing performance of the lattices, future work will need to include AgCl depletion, coating nonuniformity, gas bubble accumulation, and transient wetting behavior during long-duration operations. These effects could influence the effective wetted surface area, local mass transfer behavior, and long-term Ag^+ release stability, especially during intermittent flow or recirculated water operation.

V. Conclusion

This work demonstrates that AgCl-coated porous alumina lattices produced by Robocasting Enterprises LLC can passively dose potable water with silver ions at concentrations suitable for spacecraft water disinfection. Across multiple days of testing, two different sets of lattice samples with total AgCl loading values of 6.06 g and 5.45 g reliably produced effluent silver concentrations within the desired 200 to 400 ppb range at a flow rate of 0.1 L/min, confirming the effectiveness of this passive delivery approach. Flow rate testing showed that Ag^+ release behavior depends not only on flow dynamics but also on surface wetting, which can be influenced by the coating method. Regardless of the coating method, the lattices were able to deliver 58.4 ppb/g of AgCl at the 0.1 L/min flow rate. The computational modeling developed adds to the robustness of the experimental results by showing the nonlinear behavior of Ag^+ concentration as a function of flow rate. The model showed the outlet Ag^+ concentration decreased from 316.7 to 179.3 ppb (a 43% decrease) when the flow rate increased from 0.05 L/min to 0.25 L/min. Additionally, the model provides insight into how the rod diameter of the alumina lattice affects the outlet Ag^+ concentration. Here, increasing the rod diameter from 0.8 mm to 2.4 mm (a 300% increase) reduced the outlet Ag^+ concentration from 395 to 215 ppb (a 45.6% decrease). Overall, the results presented here support continued development of AgCl-coated lattices as a low-complexity, passive alternative to iodine-based water disinfection for future NASA missions.

VI. Acknowledgements

The authors would like to acknowledge the National Aeronautics and Space Administration (NASA) and Ames Research Center for financial support for a large portion of this work, as well as the Mars Campaign Office Life Support System Managers (Marlon Cox, Walter Schneider, Imelda Stambaugh, Michael Callahan, and Jill Williams). The authors would also like to acknowledge the technical support from the Silver Foam Team at Kennedy Space Center for their guidance on silver ISE measurement techniques and the history of silver disinfectants in potable water systems (Wenyan Li, Tesia Irwin, Angie Hanford, and Nader Azim). The porous alumina lattice structures used in this work were developed by Robocasting Enterprises LLC through NASA Small Business Innovation Research (SBIR) Phase II/IIE/III efforts supporting Environmental Control and Life Support System (ECLSS) applications under contract 80NSSC22CA117.

VII. References

[1] Y. Du, P. Liu, X. Huang, F. Meng, L. Fan, W. Li, J. Yao, X. Chen, Z. Li, M. Li, C. Lv, W. Jiang, W. Zhang, D. Sun, Prolonged Exposure to Elevated Iodine Levels in Drinking Water Is Associated With the Occurrence of Autoimmune Thyroid Disorders in Adults: Findings From a Case-Control Study Conducted in Shandong Province, China, J. Nutr. Metab. 2025 (2025) 1510663.

[2] H. Vargas-Uricoechea, A. Castellanos-Pinedo, I.A. Meza-Cabrera, M. V Pinzón-Fernández, K. Urrego-Noguera, H. Vargas-Sierra, Iodine Intake from Universal Salt Iodization Programs and Hashimoto's Thyroiditis: A Systematic Review, Diseases. 13 (2025).

[3] S.C. Bath, Thyroid function and iodine intake: global recommendations and relevant dietary trends, Nat. Rev. Endocrinol. 20 (2024) 474–486.

[4] W. Li, L.M. Calle, A.J. Hanford, I.C. Stambaugh, M.R. Callahan, Investigation of Silver Biocide as a Disinfection Technology for Spacecraft-An Early Literature Review, in: 48th Int. Conf. Environ. Syst., Albuquerque, New Mexico, 2018.
[5] M. Callahan, J. Williamson, Silver dosing technology stage gate review (SGR) evaluation criteria, 2024.
[6] NASA Administration, NASA Space Flight Human System Standard, Volume 2: Human Factors, Habitability, and Environmental Health, NASA-STD-3001 Vol. 2, 2025.
[7] T.D. Irwin, A. Diaz, L.G. Somervill, M. Hummerick, W. Li, N. Azim, Silver Foam: A Novel Approach for Long-Term Passive Dosing of Biocide in Spacecraft Potable Water Systems – Update 2025, in: 54th Int. Conf. Environ. Syst., Prague, Czech Republic, 2025.
[8] J. Cesarano, T.M. Anderson, T.J. Richardson, S. Bigham, Recent Developments For Robocast Zeolitic Lattices For Reversible CO2 Sorbent Monoliths, in: 53rd Int. Conf. Environ. Syst., Louisville, Kentucky, 2024.
[9] J. Cesarano, M. Esquibel, A. Valdez, H. Ahmadian, T.-M.J. Richardson, S. Bigham, Feasibility Assessment for Passive Silver Delivery Supported by Inorganic 3D Printed Lattice Monoliths, in: 54th Int. Conf. Environ. Syst., 2025.
[10] T.D. Irwin, W. Li, A. Diaz, L.M. Calle, M.R. Callahan, Silver Foam: A Novel Approach for Long-Term Passive-Dosing of Biocide in Spacecraft Potable Water Systems-Update 2022, in: 51st Int. Conf. Environ. Syst., St. Paul, Minnesota, 2022.
[11] W.E. Stewart, R.B. Bird, E.N. Lighfoot, Transport Phenomena, Wiley, New York, New York, 2002.
[12] N. Wakao, T. Funazkri, Effect of fluid dispersion coefficients on particle-to-fluid mass transfer coefficients in packed beds: correlation of Sherwood numbers, Chem. Eng. Sci. 33 (1978) 1375–1384.
[13] T.J. Richardson, K. Peterson, H.S. Alpert, T. Boghozian, S.J. Visser, G. Klar, Q. Dzurny, A. Schmitt, G. Sandoval, C. Ojeda, Multifunctional Sorbent (MultiSORB) Devices for Carbon Dioxide Removal, in: 52nd Int. Conf. Environ. Syst., Calgary, Canada, 2023.
[14] M. Ahmadi, S. Bigham, Gradient wick channels for enhanced flow boiling HTC and delayed CHF, Int. J. Heat Mass Transf. 167 (2021).